A comparison of I-V characteristics of graphene silicon and graphene-porous silicon hybrid structures

Haditale, M.; Zabihipour, A.; Koppelaar, H.

DOI
10.1016/j.spmi.2018.07.005

Publication date
2018

Document Version
Final published version

Published in
Superlattices and Microstructures

Superlattices and Microstructures 122 (2018) 387–393

Contents lists available at ScienceDirect

Superlattices and Microstructures

journal homepage: www.elsevier.com/locate/superlattices

A comparison of I-V characteristics of graphene silicon and graphene-porous silicon hybrid structures

M. Haditale[a,*], A. Zabihipour[b], H. Koppelaar[c]

[a] Department of Physics, Alzahra University, Tehran, Iran
[b] Adiban University, Tehran, Iran
[c] Faculty of Electrical Engineering, Mathematics and Computer Science, Delft University of Technology, Delft, The Netherlands

ARTICLE INFO

Keywords:
Semiconductors
Microporous materials
Microstructures
Raman spectroscopy
Electrical properties

ABSTRACT

A novel Graphene/Porous Silicon hybrid device is fabricated and its electrical behaviors are studied along with a Graphene/Silicon device. Graphene (G) is prepared by exfoliation of graphite foil in aqueous solution of inorganic salt. Porous Silicon (PS) is fabricated by electrochemical etching of p-type Si. Graphene is deposited on the surface of Si and PS substrates by the Thermal Spray Pyrolysis (TSP) method. The current-voltage relationships of G/Si and G/PS devices are derived and studied under different volumes of graphene. The results reveal that there are important differences in the I–V characteristics of G/Si and G/PS devices in the forward as well as reverse bias. Furthermore, varying the volume of graphene deposition on Si and PS substrates have contrary effects on their I–V characteristics.

1. Introduction

Graphene, a single layer graphite having closely packed hexagonal lattices, has received a lot of research interest due to its unique structure and fascinating properties [1,2]. The interesting properties of graphene include high thermal and electrical conductivities, excellent transparency and mechanical strength, inherent flexibility, and large specific surface area [2,3]. Due to these interesting properties are the applications of graphene emerging at a fast pace in the fields of microelectronics and optoelectronics [2,4], polymer composites [3], energy storage materials [5], and electrocatalysts [6].

Graphene can be deposited on various substrates. The two-dimensionality and structural flatness make graphene sheets ideal candidates for semiconductor materials such as Silicon (Si) [7,8], which is one of the most dominant materials in the semiconductor industry. The deposition of graphene on a substrate can effect and reduce its exclusive features and properties. Therefore, by lowering the contact surface of graphene with the substrate can reduce the effect of the substrate. A simple solution is to modify the Si wafer by using electrochemical anodization method to form Porous Silicon (PS) which has a spongy open structure and larger surface are suitable for accommodating a graphene layer on top of the pores. In Ref. [9] graphene was deposited on PS to realize stable electrodes for electromechemical devices.

Since the discovery of graphene, several methods have been devised to synthesize graphene [1]. Some of the common methods to synthesize graphene include the scotch tape method [1], chemical vapor deposition (CVD) method [10], hummers method [11,12], and electrochemical exfoliation of graphite in various electrolytic solutions [13,14].

In this research, graphene is prepared by exfoliation of graphite foil in aqueous solution of inorganic salt [14]. After the graphene

* Corresponding author.
E-mail addresses: maryam.haditale@gmail.com (M. Haditale), amir.zabihipour@adiban.ac.ir (A. Zabihipour), koppelaar.henk@gmail.com (H. Koppelaar).

https://doi.org/10.1016/j.spmi.2018.07.005
Received 23 April 2018; Received in revised form 3 July 2018; Accepted 3 July 2018
Available online 06 July 2018
0749-6036/

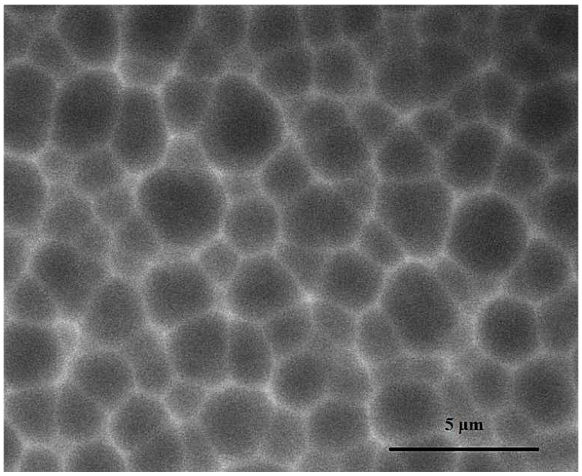

Fig. 1. SEM image of PS/Si.

powder is obtained, it is dispersed and centrifuged in dimethylformamide (DMF) solvent. Thereafter, graphene is deposited on the surface of Si and PS substrates by a Thermal Spray Pyrolysis (TSP) method. The TSP method is known for its low cost, simplicity, and possibility to be used very small size of material. To the best of our knowledge, this is the first time that by the TSP method graphene is deposited on Si and PS substrates and that its associated electrical properties are reported. Furthermore, the I–V characteristics of G/Si and G/PS devices with different volumes of graphene deposition are analyzed and compared. The most relevant prior work is [9], which differs in the method of fabrication of G/PS device and does not report our effect of volume of graphene solution on the I–V characteristics of G/PS and G/Si devices.

2. Experimental details

We used boron doped p-typed, (100) oriented Si wafers with the resistivity of 10–20 cm and thickness of 500 µm. PS was fabricated by electrochemical etching of Si wafers. Prior to the fabrication of PS, we developed an ohmic contact on the back side of the Si wafer. Electrochemical etching was performed at a constant current density of 75 mA/cm2 under one minute of etching time. The electrolyte solution contained 40% hydrofluoric acid (HF) in ethanol (99.9% Merck) with the 1:1 vol ratio. The anodization process was carried out in a homemade etching cell, where platinum (Pt) was used as cathode and an aluminum sheet pressed against the bottom of the Si wafer serves as anode. The fabricated PS sample (PS/Si sample) was finally washed in a solution of ethanol and distilled water (1:1 vol ratio) for a few seconds and then dried at room temperature. In order to study surface morphology of the fabricated PS, a SEM image was taken by TESCAN VEGA3 (cf. Fig. 1). The porosity and average pore size of the fabricated PS/Si sample are measured using Digimizer software, which are equal to 57% and 0.8 µm, respectively.

Graphene was prepared by exfoliation of graphite foil in aqueous solution of inorganic salt [14], where Pt was used as a counter cathode and graphite foil served as a working electrode (with the electrode distance of 2 cm). During the exfoliation process, the DC voltage of 10 volts was applied on the graphite electrode. After obtaining the graphene powder, 250 mg of the powder was dispersed (with 20 watts power used in the ultrasonic machine) and centrifuged in 20 ml of DMF solvent.

Graphene was deposited on Si and PS/Si substrates via TSP method at a spray rate of 0.01 ml/s and gas pressure equal to 20 psi. The distance between the nozzle and the substrate surface was equal to 11.5 cm during spraying of graphene solution. While spraying, substrates (PS and Si) temperature was kept at 100 °C to let DMF solvent evaporate from the surface of the substrates. A schematic is shown in Fig. 2.

We prepared two G/Si samples and two G/PS samples under two different volumes of graphene solution. We name these samples as G1/Si and G1/PS (prepared using 1 ml of graphene solution), and G2/Si and G2/PS (prepared using 2 ml of graphene solution). The SEM images (top views) of the G2/Si, and G1/PS samples are shown in Fig. 3. To characterize the deposited graphene, Raman spectrum measurement is performed for G1/PS device using LabRAM HR800 with the wavelength of 632.8 nm, which is shown in Fig. 4. The peaks are marked for Si, G, and G/PS.

3. Results and discussions

In this section, I–V characteristics of the fabricated G/PS and G/Si devices under different volumes of graphene solution are presented. The I–V characteristics of each device has been measured by placing one contact on one side and the other contact on the opposite side of the device, the measurements are taken across the junction.

This section is organized as follows. In Sec. 3.1 and Sec. 3.2, I–V characteristics of G/Si and G/PS devices under different volumes of graphene solution are respectively presented and analyzed. In Sec. 3.3, the comparisons are made between G/Si and G/PS devices with respect to the I–V measurements under different volumes of graphene solution.

Fig. 2. A photographic overview of set-up for our TSP method.

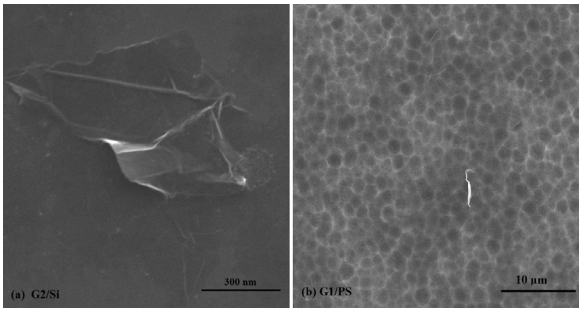

Fig. 3. SEM images of the surfaces of G2/Si and G1/PS.

3.1. I–V characteristics of G/Si devices

The I-V characteristics of G/Si devices (under 1 ml and 2 ml of graphene solution, named as G1/Si and G2/Si) are shown in Fig. 5-(a) and -(b), respectively. The fabricated G/Si devices have rectifying behavior. We recall that the I–V measurements are taken across the junctions. There are two junctions in G/Si devices: i) metal/G (high purity silver paste/G) and ii) G/Si. We propose that the rectifying behavior of G/Si devices is due to G/Si junction. The silver paste and graphene junction acts as an ohmic junction, since graphene provides an excellent conductive layer due to its semi-metal property [15]. Furthermore, Si is a p-type semiconductor and graphene has few layer structure where carbon atoms have incomplete bonds in vertical plane that are ready to make bonds. Therefore, there exists a Schottky barrier in a G/Si junction due to semi-metal role of graphene. Our observations on the Schottky barrier behavior of G/Si devices are aligned with the results reported in Refs. [7,16and17].

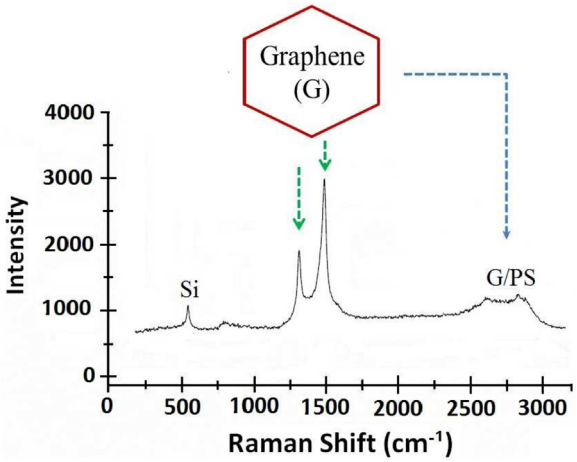

Fig. 4. Raman spectrum of G1/PS.

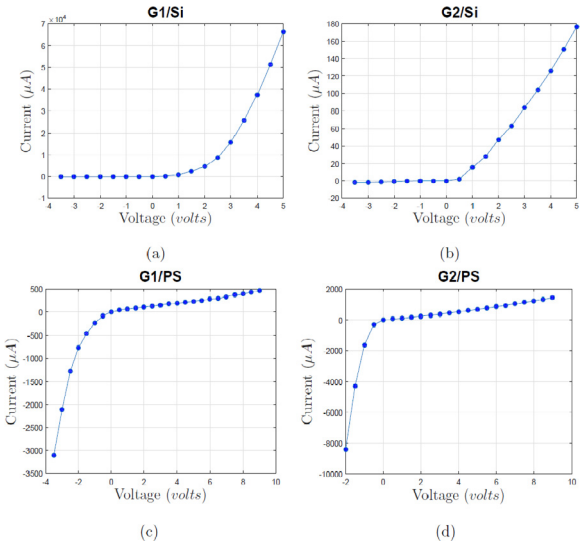

Fig. 5. I-V characteristics of the G/Si and G/PS devices.

3.1.1. Effect of varying volume of graphene solution on Si

According to Fig. 5-(a) and -(b), the current measurements in G1/Si device are higher than the current measurements in G2/Si device for all voltage values. When lower volume of graphene solution is sprayed on Si, it leads to low layer graphene. The structure of the low layer graphene on the substrate is regular and well-ordered. We assume that the well-ordered structure is similar to the "ABAB · · ·" structure of graphene that is supposed to be more conductive [18]. But when higher volume of the graphene solution is deposited on Si, the structure of graphene is less ordered and is similar to the "ABCABC · · ·" structure of graphene that has lower conductivity [18].

In accordance with Fig. 5, knee points in the I-V curves of G1/Si and G2/Si devices occur at (2 volts, 4610 μA) and (1 volt, 15.7 μA), respectively. It is interesting that although the current values in G1/Si are higher than that of G2/Si, the threshold voltage (≈2 volts) in G1/Si is higher than the threshold voltage (≈1 volt) in G2/Si.

3.2. I–V characteristics of G/PS devices

The I–V characteristics of G/PS devices (fabricated using 1 ml and 2 ml of graphene solution, named as G1/PS and G2/PS) are shown in Fig. 5-(c) and -(d), respectively. In G/PS devices (while taking I–V characteristics across the junction), there are three junctions including metal/G (high purity silver paste/G), G/PS, and PS/Si. As discussed earlier, metal/G behaves as an ohmic junction. Hence, there are two effective junctions including G/PS and PS/Si junctions. The PS/Si junction has diodic behavior due to the quantum confinement that comes from the porosity in the PS side [19]. For the G/PS junction, we propose that it behaves as a Schottky barrier due to graphene deposited on spongy surface of PS which is fabricated from a p-type Si wafer. Since graphene has a

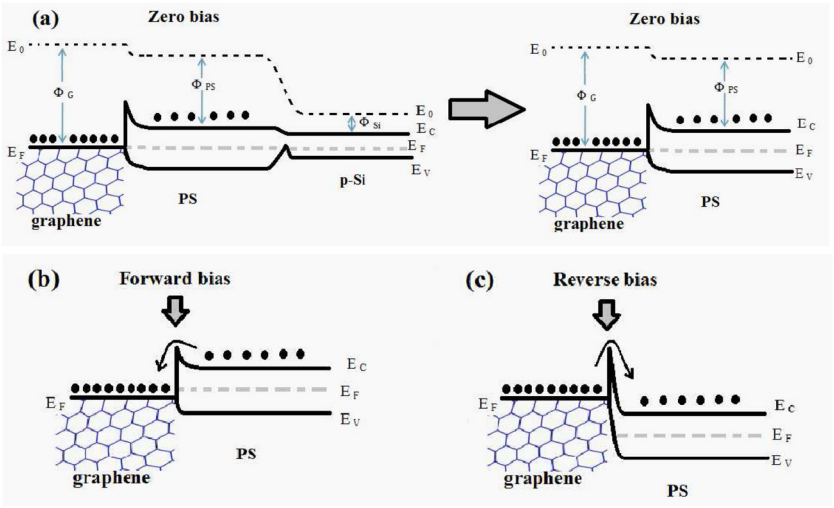

Fig. 6. Schematic of energy band diagrams; (a) zero bias of G/PS device and G/PS junction, (b) forward bias of G/PS junction, (c) reverse bias of G/PS junction.

semi-metal role with excellent conductivity and high electron mobility, the behavior of G/PS device is mainly dominated by G/PS junction. The effect of the diodic junction of PS/Si on the behavior of the G/PS device is further discussed in Sec. 3.2.1.

The I-V curves reveal that the current values in the reverse bias of the G/PS devices are higher than those in the forward bias, i.e., the current values rise relatively sharply in the reverse bias. This observation can be explained as follows. The behavior of the G/PS devices is dominated by G/PS Schottky junction, as discussed earlier. The band gap in the PS side of the PS/Si junction increases due to quantum confinement. The increase in the band gap creates a potential barrier that causes a rectifying behavior. Further, there exist atoms in PS side with incomplete links on the surface of the PS/Si device, which leads to n-type role of the PS with respect to Si. Moreover, each carbon atom in graphene structure has incomplete bonds in the vertical plane which are ready to complete bonds. Hence, we hypothesize that in the G/PS Schottky junction, there is an interface of semi-metal structure of graphene and n-type role of the PS. As known for the Shottky barriers, current transport is done by the majority charge carriers and electrons are majority carriers in both graphene and PS. In Fig. 6, a schematic of the energy band diagrams illustrating the mechanisms of G/PS junction in both biases, is shown. Graphene has a greater number of electrons than PS, since in graphene there is an incomplete bond per carbon atom and in PS are the links in some of the Si atoms broken due to the increased surface to volume ratio. In forward bias, energy levels are such that the electrons (majority carriers in G/PS Schottky junction) can easily flow from PS to graphene, whereas in reverse bias electrons can easily move from graphene to PS side. Since the population of the electrons in graphene is larger with high electron mobility, the current values in the reverse bias are higher than those in the forward bias.

3.2.1. Effect of graphene deposition on PS

Fig. 7 shows a comparison of the I–V measurements in PS/Si and G/PS devices. The current values in G/PS devices are higher than that of PS/Si device. The high percentage of porosity (57%) in the PS/Si device causes a large disorder in the PS tissue due to the large pore size, which creates lesser Si environment for the movement of electrons on the PS side. The pores provide resistance and the

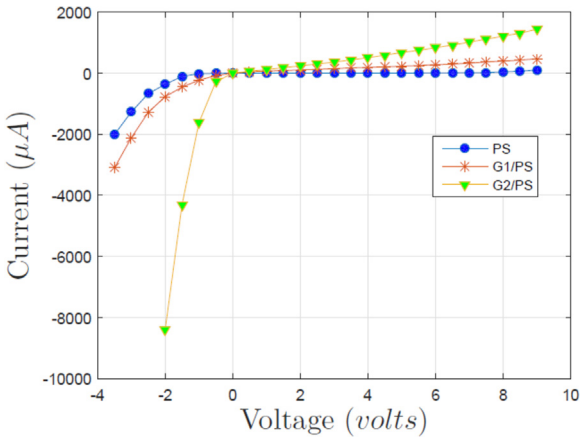

Fig. 7. A comparison of I–V characteristics of PS/Si and G/PS devices.

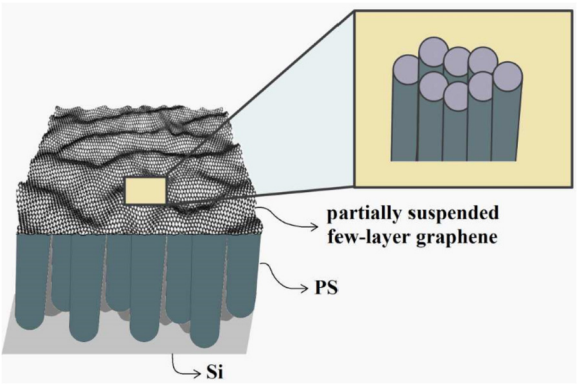

Fig. 8. Schematic of graphene layer on top of the PS surface in G/PS device.

current measurement reduce in the PS/Si device. However, after the deposition of graphene layer on PS surface, an enhancement in currents is observed. We propose that this enhancement in current is due to the following reasons:

(1) Since the graphene solution is centrifuged before spraying, the large sized flakes of the graphene are settled as residue in solution and the small sized flakes of graphene exist in the solution. The pores in the PS surface are large enough (average pore size is 0.8 μm) to accommodate tiny sized flakes of graphene (average size of graphene flakes is 0.5 μm). This conclusion is reasonable since PS has active surface due to the porosity. Thus, the diodic PS/Si junction affected by an excellent conductivity of penetrated graphene flakes improves current transmission.
(2) The porosity breaks the links between some atoms on the surface, i.e., there exist atoms with incomplete links on the surface of the PS/Si device that makes the surface of the PS as an active surface [19]. On the other hand, each of the carbon atom in graphene makes three electron bonds with neighboring atoms in horizontal plane and the forth electron is free on vertical plane, ready to make a bond. Thus, by deposition of graphene on PS surface, some of the incomplete atoms in graphene and PS can make bonds, leading to improvement in transmitted currents.
(3) – According to the SEM images (cf. Fig. 3b), the few layers of graphene act as an ultrathin netting with the excellent conductivity on top of the PS surface, joining the walls of the pores. The high conductive graphene layer on the top of pores enhances transmission of electrons and overcome the resistance that is due to less Si environment. In Fig. 8, a schematic of graphene layer on top of a PS layer is illustrated.

3.2.2. Effect of varying volume of graphene on PS

G2/PS device gives higher current measurements than G1/PS, according to the measured I–V curves. The reason is that graphene solution is centrifuged, i.e., the solution is rarefied and therefore a higher density of graphene flakes in G2/PS device can result in higher penetration of graphene flakes into the porous surface and also better covering of the porous surface by the graphene flakes. The higher penetration and the improved covering of graphene flakes on the PS surface leads to improved conductivity. To study this further, the current measurements in G1/PS and G2/PS at 9 volts and −1 volts are given in Table 1. We note that by increasing the graphene volume from 1 ml to 2 ml at 9 volts, the current in the G/PS devices becomes three-folds and the ratio of current measurement in the G/PS device to the current measurement in the PS/Si device increases from 4.3 to 13.2 (by increasing graphene volume). Similar observation can be made in reverse bias, where current in the G/PS device increases almost 7 times by increasing the graphene volume from 1 ml to 2 ml at −1 volts. Furthermore, the ratio of current measurement in the G/PS device to the current measurement in the PS/Si device increases from 12.4 to 87.5 at −1 volts. As mentioned earlier and discussed here, the current values in the reverse bias are much greater than in the forward bias.

3.3. Comparing I–V characteristics of G/Si and G/PS devices

There is a significant difference in the I–V characteristics of the G/Si and the G/PS devices (cf. Fig. 5). The I–V curves of the G/PS devices rise sharply and have lower knee voltages (turn on voltages) compared to the I–V curves of the G/Si devices in the forward bias. In the reverse bias, the current values are approximately zero in the G/Si devices in contrast to G/PS devices that have

Table 1
Comparison of current measurements.

Current at −1 volts	Current at 9 volts	Samples
−18.5 μA	108.5 μA	PS/Si
−230 μA	468.5 μA	G1/PS
−1620 μA	1437 μA	G2/PS

considerable current values. The differences in the I–V behaviors of G/Si and G/PS devices can be referred to different effective Schottky barriers in these devices. As discussed in Sec. 3.1 and Sec. 3.2, in the G/Si devices there is one effective junction (G/Si Schottky junction) that behaves as rectifier, whereas in the G/PS devices, there are two effective junctions: G/PS Schottky junction and the diodic PS/Si junctions. We suggest that it is mainly the porosity that creates the difference in I–V relationships of the two devices. The pores in the PS surface are large enough (0.8 μm on average) to accommodate tiny sized (0.5 μm on average) flakes of graphene. Furthermore, there is a partially suspended graphene layer on top of the PS surface, as illustrated in Fig. 8. Thus, the penetration of graphene in the pores of the substrate as well as the partially suspended graphene layer on the substrate enhances the current transmission and electrical conductivity.

It is also important to note that the current values in the G/Si devices decrease with increase in graphene volume (from 1 ml to 2 ml) unlike the G/PS devices where the current values increase with the increase in graphene volume. Considering forward bias, the current measurements in G1/Si are higher than in G1/PS, whereas the current measurements in G2/Si are lower than in G2/PS. The reasons for these behaviors have been discussed earlier in Sec. 3.1.1 and Sec. 3.2.2.

4. Conclusions

There are significant differences in the I-V characteristics of the G/Si and G/PS devices in the forward as well as reverse bias. In the forward bias, the I-V curves of the G/PS devices rise sharply and have lower knee points compared to the I-V curves of the G/Si devices. In the reverse bias, the current values are approximately zero in the G/Si devices in contrast to the G/PS devices that have very large current values. Interestingly, an increase in the volume of graphene solution enhances current in the G/PS devices, whereas it reduces current in the G/Si devices. The differences in the I–V behaviors of the G/Si and G/PS devices are due to different effective Schottky barriers in these devices and it is mainly the porosity that creates the difference. Further, it is observed that the deposition of graphene on PS substrate boosts the current transmission in both reverse and forward bias. The PS/Si device has a rectifier behavior significantly different from that of the G/PS device. For the G/PS device, the current values in the reverse bias are much greater than the current values in the forward bias.

References

[1] K.S. Novoselov, A.K. Geim, S.V. Morozov, D. Jiang, Y. Zhang, S.V. Dubonos, I.V. Grigorieva, A.A. Firsov, Electric field effect in atomically thin carbon films, Science 306 (2004) 666–669.
[2] K.S. Novoselov, A.K. Geim, The rise of graphene, Nat. Mater. 6 (2007) 183–191.
[3] Y. Sun, Q. Wu, G. Shi, Graphene based new energy materials, Energy Environ. Sci. 4 (2011) 1113–1132.
[4] F. Bonaccorso, Z. Sun, T. Hasan, A.C. Ferrari, Graphene photonics and optoelectronics, Nat. Photon. 4 (2010) 611–622.
[5] M.D. Stoller, S. Park, Y. Zhu, J. An, R.S. Ruoff, Graphene-based ultracapacitors, Nano Lett. 8 (2008) 3498–3502.
[6] H. Bai, Y. Xu, L. Zhao, C. Li, G. Shi, Non-covalent functionalization of graphene sheets by sulfonated polyaniline, Chem. Commun. (2009) 1667–1669.
[7] X. Li, H. Zhu, K. Wang, A. Cao, J. Wei, C. Li, Y. Jia, Z. Li, X. Li, D. Wu, Graphene-on-silicon Schottky junction solar cells, Adv. Mater. 22 (2010) 2743–2748.
[8] H. Xiang, K. Zhang, G. Ji, J.Y. Lee, C. Zou, X. Chen, J. Wu, Graphene/nanosized silicon composites for lithium battery anodes with improved cycling stability, Chem. Commun. 49 (2011) 1787–1796.
[9] L. Oakes, A. Westover, J.W. Mares, S. Chatterjee, W.R. Erwin, R. Bardhan, S.M. Weiss, C.L. Pint, Surface engineered porous silicon for stable, high performance electrochemical supercapacitors, Sci. Rep. 3 (2013) 3020–3027.
[10] H.J. Park, J. Meyer, S. Roth, V.S. Kalova, Growth and properties of fewlayer graphene prepared by chemical vapor deposition, Carbon 48 (2010) 1088–1094.
[11] G. Wang, J. Yang, J. Park, X. Gou, B. Wang, H. Liu, J. Yao, Facile synthesis and characterization of graphene nanosheets, J. Phys. Chem. C 112 (2008) 8192–8195.
[12] K. Muthoosamy, R.G. Bai, I.B. Abubakar, S.M. Sudheer, H.N. Lim, H.S. Loh, N.M. Huang, C.H. Chia, S. Manickam, Exceedingly biocompatible and thin-layered reduced graphene oxide nanosheets using an eco-friendly mushroom extract, Int. J. Nanomed. 10 (2015) 1505–1519.
[13] K. Parvez, R. Li, S.R. Puniredd, Y. Hernandez, F. Hinkel, S. Wang, X. Feng, K. M¨ullen, Electrochemically exfoliated graphene as solutionprocessable, highly conductive electrodes for organic electronics, Am. Chem. Soc. 7 (2013) 3598–3606.
[14] K. Parvez, Z.S. Wu, R. Li, X. Liu, R. Graf, X. Feng, K. M¨ullen, Exfoliation of graphite into graphene in aqueous solutions of inorganic salt, J. Am. Soc. 136 (2014) 6083–6091.
[15] R.S. Dariani, M. Haditale, E. Ghasemian, Electrical behavior of graphene under temperature effect and survey of I-T curve, Semiconductors (2017) (Submitted).
[16] Z. Liang, X. Cai, S. Tan, P. Yang, L. Zhang, X. Yu, K. Chen, H. Zhu, P. Liu, W. Mai, Fabrication of n-type zno nanowire/graphene/p-type silicon hybrid structures and electrical properties of heterojunctions, Phys. Chem. Chem. Phys. 14 (2012) 16111–16114.
[17] V.V. Brus, M.A. Gluba, X. Zhang, K. Hinrichs, J. Rappich, N.H. Nickel, Stability of graphenesilicon heterostructure solar cells, Phys. Status Solidi A 211 (2014) 843–847.
[18] P. Serp, B. Machado, Nanostructured carbon materials for catalysis, RSC catalysis series no. 23, Roy. Soc. Chem. (2015).
[19] R.S. Dariani, M. Zabihipour, Effect of electrical behavior of zno microparticles grown on porous silicon substrate, Appl. Phys. A (2016).